Molecular Crystals and Liquid Crystals
Publication details, including instructions for authors and subscription information:
http://www.tandfonline.com/loi/gmcl16

Thermodynamic Properties of Ferrocene Crystal

Kouji Ogasahara [b a], Michio Sorai [a] & Hiroshi Suga [a]

[a] Department of Chemistry and Chemical Termodynamics Laboratory, Faculty of Science, Osaka University, Toyonaka, Osaka, 560, Japan

[b] Intergrated Circuit Section, Shart Corporation, Tenri, Nara, 632, Japan

Version of record first published: 20 Apr 2011.

To cite this article: Kouji Ogasahara , Michio Sorai & Hiroshi Suga (1981): Thermodynamic Properties of Ferrocene Crystal, Molecular Crystals and Liquid Crystals, 71:3-4, 189-211

To link to this article: http://dx.doi.org/10.1080/00268948108072321

Mol. Cryst. Liq. Cryst., 1981, Vol. 71, pp. 189–211
0026-8941/81/7104-0189/$06.50/0

Printed in the United States of America

Thermodynamic Properties of Ferrocene Crystal†

KOUJI OGASAHARA,‡ MICHIO SORAI and HIROSHI SUGA

Department of Chemistry and Chemical Thermodynamics Laboratory, Faculty of Science, Osaka University, Toyonaka, Osaka 560, Japan

(*Received September 11, 1980*)

The heat capacities of ferrocene crystals have been measured between 13 and 300 K for large and powdered crystals. The phases studied include the triclinic metastable low-temperature (LT) phase, the monoclinic high-temperature (HT) phase, the orthorhombic stable LT-phase and also the undercooled HT- and the superheated orthorhombic LT-phases. The enthalpy and entropy of the λ-type transition from the metastable LT- to the undercooled HT-phase at 163.9 K and the first order transition from the stable LT- to the HT-phase at 242 K have been determined. The latter phase transition is concluded to be characterized by softening of a translational mode along the crystallographic "*c*-axis." The influence of crystal size is reflected in the shape of the heat capacity curve in the vicinity of the λ-point whereas the transition enthalpy and entropy are identical regardless of crystal size. The disintegration phenomenon of large ferrocene crystal may be interpreted in terms of a change in the state on a *P-H-T* surface.

1 INTRODUCTION

Bis(η-cyclopentadienyl)iron $Fe(C_5H_5)_2$, commonly called ferrocene, has been the interesting subject of experimental and theoretical works in the last three decades. However, in spite of its simple molecular structure, there remain many questions still unanswered as to the physicochemical properties of ferrocene crystal. First of all, the mechanism of the well-known λ-type phase transition at 163.9 K found by Edwards *et al.*[1,2] is to be reconsidered because the molecular and crystal structures of both phases below and above the λ-point so far widely believed[3–5] should be revised in the light of recent structural reinvestigation.[6–11]

Moreover, our finding[12] of a new low-temperature (LT) phase, which exists stably in the thermodynamic sense below 242 K, seems to be one of the impor-

† Contribution No. 11 from Chemical Thermodynamics Laboratory.
‡ Present address: Integrated Circuit Section, Sharp Corporation, Tenri, Nara 632, Japan.

tant results in ferrocene science; the λ-transition hitherto known[1] turned out to be a transition between metastable phases. This was quite recently confirmed by X-ray diffraction analysis;[13] the stable LT-phase belongs to an orthorhombic system in contrast to the triclinic system of the metastable LT-phase and the monoclinic one of the high-temperature (HT) phase. One of the purposes of the present paper is to present exact phase relationship and the nature of the stable LT-phase from a thermodynamic point of view.

In addition to the existence of many crystalline phases, a shattering phenomenon of ferrocene crystal[14] makes the situation rather complicated. When large crystals of ferrocene are cooled below the λ-point, they undergo a violent disintegration into a powder. Since the disintegration is accompanied by a large quantity of heat evolution, it is expected that large ferrocene crystals might store a considerable amount of strain energy in their crystal lattice at low temperatures in comparison with shattered crystallites.[12,14] We were interested in the effects exerted by the strain energy on the thermodynamic properties of ferrocene crystal. We measured the heat capacities of both the large and powdered crystals and determined the enthalpy relationship between them. Discussion of these problems is also one of the present purposes.

2 EXPERIMENTAL

Sample preparation

Preparation of large ferrocene crystals has been described previously.[12] The crystals were put through sieves with mesh-sizes 1.30, 0.840, 0.351, 0.246 and 0.105 mm to obtain four kinds of narrow sieve fractions. The disintegration phenomenon was examined for these four sieve fractions, while only the fraction 0.840–1.30 mm was used for the heat capacity measurements.

Thermal analyses

Crystal size dependence of the disintegration phenomenon was examined by a differential thermal analysis (DTA) apparatus.[15] The amount of specimen required for this apparatus is about 200–300 mg. In order to check whether the enthalpy difference exists between the large and powdered crystals even at higher temperatures, the heat of fusion was measured for both samples by a differential scanning calorimeter (DSC; Du Pont Model 990).

Heat capacity measurements

The heat capacities were measured between 13 and 300 K with an adiabatic-type calorimeter.[16] A new calorimeter cell suitable for the present purpose was constructed (Figure 1). The cell is made of gold-plated copper with 0.3 mm in thickness except for lid and flange (1.0 mm). The cylinder is 30 mm in diame-

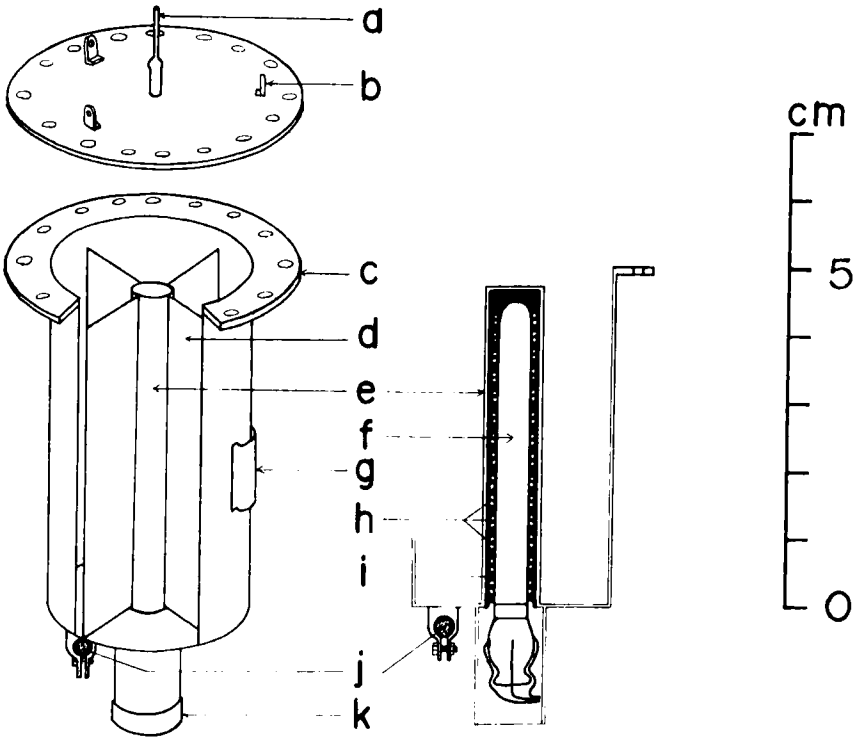

FIGURE 1 Cross-sectional diagrams of the calorimeter cell. (a) capillary for exchange gas, (b) ring for hook, (c) flange, (d) vane, (e) re-entrant well for thermometer and heater, (f) capsule-type platinum resistance thermometer, (g) differential thermocouple sleeve, (h) Nylon-insulated wire for heater, (i) Wood's alloy, (j) capsule-type germanium resistance thermometer and (k) cap for re-entrant well.

ter, 50 mm in depth and *ca.* 30 cm^3 in volume. A demountable lid allows the container to be easily loaded with any samples regardless of crystal size. The vacuum tightness of the cell can be achieved by an indium gasket with 0.5 mm in diameter between the flange and the lid. After evacuation of air from the cell, a small amount of helium gas is introduced through a capillary (*a*) into the cell as a heat exchanger and the entrance of the capillary is soldered. The temperature of the cell assembly can be measured with a platinum resistance thermometer (*f*; Leeds & Northrup) in the range 13 to 300 K and with a germanium resistance thermometer (*j*; Cryo Cal, Inc.) between 1.5 and 20 K. The temperature scale above 13 K has been calibrated based on the IPTS-68. The heater wire (*h*) is double-Nylon-insulated Karma wire (Driver Harris Co.) with a resistance of *ca.* 100 Ω.

To perform a variety of measurements, we loaded four times the calorimeter cell with freshly prepared ferrocene crystals with the sieve fraction 0.840–1.30 mm. We shall hereafter designate them as sample-I, II, III and IV,

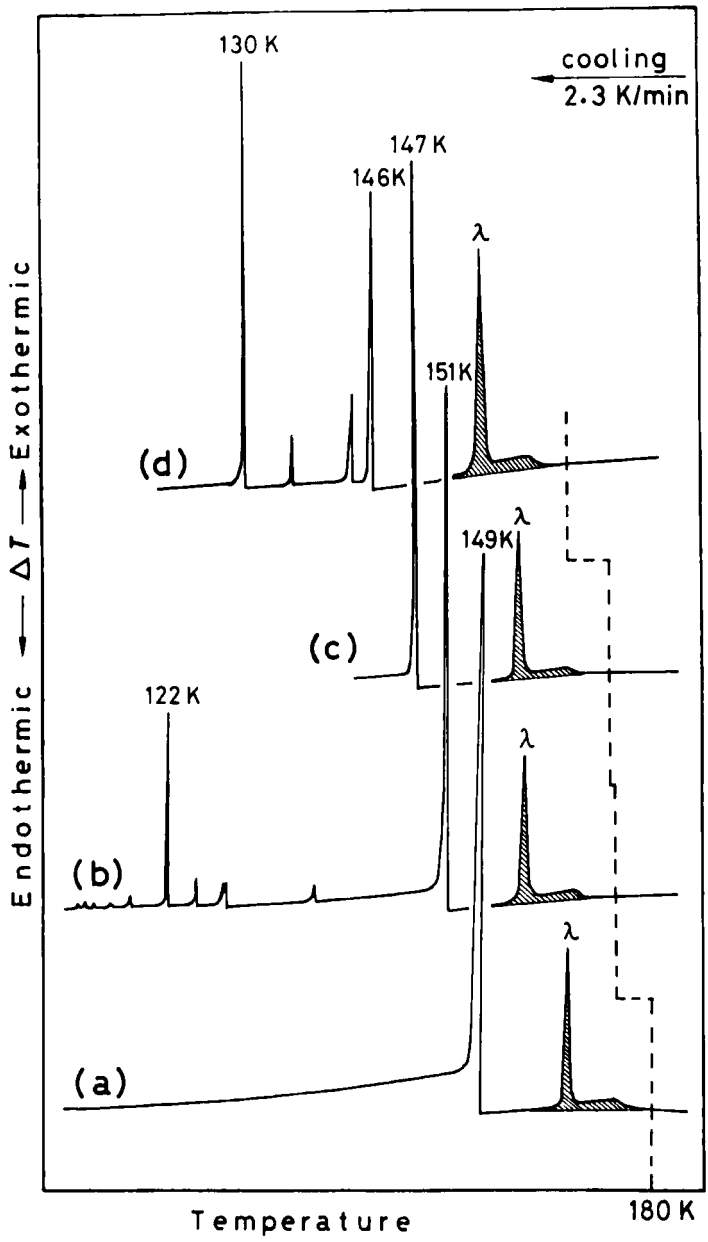

FIGURE 2 DTA curves with a cooling rate of 2.3 K min^{-1} for four sieve fractions of ferrocene crystal; (a) 1.30–0.840 mm, (b) 0.840–0.351 mm, (c) 0.351–0.246 mm and (d) 0.246–0.105 mm. The abscissas are shifted for better illustration. The λ-transition at 163.9 K and the subsidiary peak at 169 K are shaded in order to distinguish them from the disintegration peaks.

respectively. The amount of the sample used was 21.0527 g (≙ 0.113165 mol) for sample I, 20.9383 g (≙ 0.112550 mol) for sample II and 21.1809 g (≙ 0.113854 mol) for sample III and IV.

3 RESULTS

Disintegration phenomenon

Figure 2 shows the DTA curves recorded with a cooling rate of 2.3 K min^{-1} for the four sieve fractions; (a) 1.30–0.840 mm, (b) 0.840–0.351 mm, (c) 0.351–0.246 mm and (d) 0.246–0.105 mm. When the crystals were cooled below the λ-point, a dominant exothermic peak arising from violent disintegration into a powder was observed in the range 146 to 151 K. In general, small successive peaks due to further fracturing followed at lower temperatures. This seems to be resulted from the fact that the present DTA apparatus[15] requires a large specimen, as much as 200–300 mg, and thus it is difficult for the disintegration to occur simultaneously. If we could examine the shattering phenomenon by using one piece of crystal, a single-step disintegration would be expected. In fact, the shattering phenomenon did occur at a single temperature in an "ideal" case shown in Figure 2(a). It should be remarked that the heat evolution due to the release of strain energy stored in the crystals is much larger than the enthalpy of the λ-transition. Contrary to our expectation, the disintegration temperatures were approximately identical regardless of the crystal size at least in the rage 0.105–1.30 mm. However, it remains true that extremely small crystallites do not exhibit the disintegration as the powdered specimen pulverized by an agate mortar did not show any peaks down to liquid nitrogen temperature. The crystal size dependence of the distintegration phenomenon should, therefore, be examined for smaller crystals than 0.105 mm.

It is relevant to note here that Bodenheimer and Low[14] have reported much lower disintegration temperature of 108–125 K. Since there are no descriptions of the crystal sizes and the experimental details in their report, we cannot directly compare their results with ours. The disintegration temperature is known to depend at least on a cooling rate and pressure,[14] and probably on preparation methods of large crystals as well. The previous authors[14] grew the single crystals from solution of toluene and other solvents, while we prepared them by slow sublimation.[12] The large difference between the two sets of the results seems to be caused by these different experimental conditions.

Heat capacities

The results of the calorimetric measurements are listed in Table I. Ferrocene crystal exhibits various phases according to the thermal history of the sample

as well as the crystal size. In Table I, therefore, each series of measurements is indicated by both the relevant phase(s) and the particle size. As to the former, the following abbreviations are employed; (monoclinic) stable HT-phase (sHT for short), undercooled HT-phase (ucHT), (triclinic) metastable LT-phase (msLT), (orthorhombic) stable LT-phase (sLT) and superheated LT-phase (shLT), respectively. On the other hand, as to the particle size, the symbol "A" means the large crystals of the sieve fraction 0.840–1.30 mm, "B" is

TABLE I

Molar heat capacity of ferrocene crystal

T_{av}/K	C_p/J K^{-1} mol^{-1}	T_{av}/K	C_p/J K^{-1} mol^{-1}	T_{av}/K	C_p/J K^{-1} mol^{-1}
Sample I		251.78	158.57	163.06	125.87
ΔH[disintegration		254.62	160.49	163.71	506.95
at 154.4 K; msLT		257.60	162.48	164.09	557.17
(A→C*)]		260.56	164.43	164.72	128.43
Sample II		263.50	166.35	165.61	125.56
{msLT(A), ucHT(A)}		266.41	168.32	166.50	126.29
162.15	122.62	269.31	170.31	167.51	126.70
162.73	124.39	272.19	172.36	168.73	127.93
163.50	155.63	275.05	174.05	170.05	129.46
163.89	6843.1	277.89	175.96	ΔH[stabilization;	
164.22	214.41	280.71	177.77	ucHT(A)→sLT(B)]	
164.95	125.42	283.51	179.62		
165.79	125.77	286.29	181.49	Series 4	
166.84	126.42	289.40	183.82	{sLT(B), shLT(B)}	
168.10	127.32	292.81	186.08	159.26	99.87
169.35	128.72	296.21	188.15	160.70	100.61
170.59	130.27	Series 2		162.12	101.44
171.82	132.68	{ucHT(A)}		163.54	102.26
Sample III		166.99	125.93	164.96	103.04
Series 1		168.28	127.53	166.36	103.84
{ucHT(A), sHT(A)}		169.57	129.04	167.76	104.69
210.35	133.51	170.84	131.05	169.16	105.54
212.59	134.75	172.10	134.05	170.54	106.32
214.82	135.95	173.37	126.87	171.92	107.22
217.03	137.20	174.66	123.21	173.29	108.00
219.23	138.44	175.95	121.98	175.20	109.08
221.42	139.69	177.25	121.06	177.66	110.61
223.60	141.00	179.30	120.87	180.10	112.08
225.76	142.28	ΔH[ucHT(A, 179 K)→		182.51	113.63
227.91	143.50	sHT(A, 258 K)]		184.91	115.12
230.05	144.82	{sHT(A)}		187.29	116.57
232.18	146.06	257.65	162.41	189.65	118.05
234.29	147.38	259.57	163.85	191.99	119.64
236.40	148.60	260.93	164.79	194.32	121.09
238.49	149.99	Series 3		196.63	122.54
240.91	151.48	{msLT(A)}		198.92	124.06
243.67	153.29	160.32	117.91	201.20	125.61
246.40	155.13	161.24	119.71	203.46	127.08
249.09	156.76	162.15	122.18	205.71	128.58

TABLE I (*continued*)

Molar heat capacity of ferrocene crystal

T_{av}/K	C_p/J K^{-1} mol^{-1}	T_{av}/K	C_p/J K^{-1} mol^{-1}	T_{av}/K	C_p/J K^{-1} mol^{-1}
207.94	130.07		Series 6		ΔH[transition;
210.15	131.61		{sLT(B)}		sLT(B)→sHT(B)}
212.36	133.11	87.44	64.26		{sHT(B)}
214.54	134.60	88.98	65.14	257.07	161.80
216.72	136.13	90.88	65.99	259.96	163.78
218.88	137.64	92.74	66.87	262.83	165.75
221.03	139.04	94.57	67.71	265.69	167.62
223.16	140.58	96.37	68.60	268.52	169.54
225.28	142.05	98.15	69.40	272.73	172.40
227.38	143.58	99.90	70.22	276.91	174.92
229.46	145.15	101.81	71.05		(rapid cooling)
231.53	146.66	103.85	72.04		Series 7
233.59	148.14	105.87	73.00		{msLT(C)}
235.64	149.64	107.87	73.88	14.44	9.06
237.67	151.14	109.83	74.82	15.13	10.06
239.69	152.58	111.78	75.75	15.91	11.12
241.70	154.11	113.70	76.62	16.72	12.23
243.69	155.58	115.60	77.50	18.19	14.22
245.68	157.02	117.48	78.41	19.11	15.49
247.66	158.55	119.15	79.17	20.17	17.00
	{sHT(B)}	120.87	79.96	21.38	18.62
259.46	163.35	122.82	80.87	22.60	20.25
262.41	165.78	124.74	81.87	23.71	21.73
265.33	168.26	126.65	82.78	24.83	23.16
268.24	169.98	128.54	83.72	25.97	24.53
271.12	171.83	130.42	84.69	27.18	26.09
273.99	173.61	132.27	85.58	28.47	27.60
276.84	175.29	134.11	86.61	29.77	29.07
279.67	177.17	135.94	87.47	31.16	30.63
282.48	178.87	137.75	88.36	32.64	32.23
285.27	180.76	139.77	89.42	34.23	33.87
288.05	182.73	141.99	90.51	35.85	35.48
290.80	184.89	144.19	91.70	37.35	36.95
293.99	186.76	146.38	92.84	38.78	38.28
297.61	189.20	148.54	93.90	40.18	39.44
		150.69	95.09	41.60	40.68
	Series 5	152.81	96.26	43.02	41.81
	{msLT(B),ucHT(B)}	154.93	97.40	44.40	42.87
156.68	111.12	157.02	98.55	45.79	43.97
157.81	113.25	159.10	99.72	47.33	45.15
159.29	116.15	160.77	100.46	47.89	45.59
160.76	120.20	162.28	101.47	49.47	46.73
162.18	130.46	163.78	102.29	50.99	47.80
163.42	222.70	165.69	103.39	52.45	48.74
164.46	249.90	229.50	144.99	53.87	49.65
165.63	145.81	232.57	147.21	55.24	50.53
166.99	128.66	235.60	149.34	56.57	51.34
	ΔH[stabilization;	238.12	150.77	58.02	52.22
	ucHT(B)→sLT(B)}	240.14	152.44	59.59	53.13

TABLE I (*continued*)

Molar heat capacity of ferrocene crystal

T_{av}/K	C_p/J K^{-1} mol^{-1}	T_{av}/K	C_p/J K^{-1} mol^{-1}	T_{av}/K	C_p/J K^{-1} mol^{-1}
61.09	53.88	69.44	55.38	Series 9 {msLT(C)}	
(stabilization)		71.01	56.24	150.79	104.98
Series 8 {sLT(C)}		72.64	57.08	152.21	106.42
12.52	3.80	74.28	57.95	153.62	108.02
13.66	5.02	75.93	58.91	155.02	109.60
14.70	6.13	77.55	59.65	156.40	111.44
15.67	7.18	79.13	60.47	157.78	113.39
16.50	8.12	80.69	61.18	159.13	115.68
17.28	9.02	82.32	61.94	160.48	118.62
18.04	9.93	84.01	62.80	161.80	123.25
18.81	10.87	85.67	63.62	163.07	141.97
19.65	11.96	87.58	64.50	164.07	335.90
20.50	12.96	89.72	65.55	164.99	188.54
21.30	13.96	{sLT(C)}		166.14	141.93
22.17	15.05	162.09	101.54	ΔH {stabilization; ucHT(C)→sLT(C)}	
23.19	16.31	163.33	102.17		
24.30	17.71	164.57	102.84		
25.47	19.14	{sLT(C),shLT(C)}			
26.71	20.69	211.13	132.15		
27.94	22.16	213.27	133.67	Series 10 {sLT(C)}	
29.08	23.52	215.40	135.17	236.10	149.60
30.14	24.70	217.51	136.60	238.13	151.12
31.26	25.98	219.60	138.08	240.14	152.61
32.53	27.37	223.24	140.65	ΔH {transition; sLT(C)→sHT(C)}	
33.93	28.88	226.85	143.18		
35.34	30.36	228.89	144.65		
36.74	31.81	230.92	146.10		
38.23	33.27	232.94	147.44		
39.73	34.68	234.95	148.97		
41.20	36.00	236.94	150.35	{sHT(C)}	
42.67	37.28	238.93	151.82	262.41	165.61
44.13	38.52	240.87	153.07	Series 11 {ucHT(C),sHT(C)}	
45.57	39.72	242.86	154.78	228.52	143.73
46.99	40.90	244.84	156.52	230.57	144.94
48.52	42.08	ΔH {transition; shLT(C)→sHT(C)}		232.61	146.14
50.13	43.36			234.65	147.40
50.93	43.90			236.67	148.61
52.44	44.97	{sHT(C)}		238.68	149.94
53.98	46.04	262.94	166.09	240.69	151.14
55.55	47.09	265.78	167.93	242.68	152.43
57.16	48.16	268.60	169.73	244.66	153.75
58.80	49.20	271.40	171.69	247.12	155.37
60.34	50.11	274.14	173.32	250.06	157.35
61.88	51.12	276.90	175.17	252.97	159.29
63.38	51.95	279.64	177.04	255.87	161.18
64.93	52.82	282.36	178.85	258.74	163.06
66.54	53.82	285.07	180.66	261.60	164.99
68.10	54.68	287.75	182.50		

TABLE I (*continued*)

Molar heat capacity of ferrocene crystal

T_{av}/K	C_p/J K^{-1} mol^{-1}	T_{av}/K	C_p/J K^{-1} mol^{-1}	T_{av}/K	C_p/J K^{-1} mol^{-1}
Series 12 {msLT(C)}		272.90	172.45	73.08	60.43
		275.90	174.40	74.43	61.06
100.95	73.67	278.88	176.57	75.77	61.83
103.14	74.80	281.84	178.50	77.21	62.45
105.30	75.91	284.78	180.39	78.75	63.24
107.42	76.96	287.69	182.50	80.27	63.91
109.51	78.07	Series 14 {ucHT(C)}		81.76	64.63
111.58	79.10				
113.62	80.16	220.87	139.10		
115.64	81.18	222.75	140.24		
117.63	82.26	224.63	141.34	*Sample IV* (slow cooling down to 10.5 K and rewarming to 288 K)	
119.60	83.30	226.50	142.51		
121.55	84.44	228.35	143.62		
123.02	85.11	Series 15 {ucHT(C)}			
124.54	86.04			Series 1 {msLT(B + C*), ucHT(B + C*)}	
126.55	87.25	208.17	131.72		
128.67	88.55	Series 16 {msLT(C)}			
130.88	89.90			153.60	108.16
133.06	91.29	80.75	64.14	155.27	110.18
135.23	92.79	82.66	65.12	157.15	112.71
137.37	94.22	84.54	66.06	159.00	115.91
139.48	95.73	86.38	66.96	160.83	120.51
141.58	97.24	88.22	67.81	162.38	130.93
143.65	98.88	90.07	68.67	163.47	286.79
145.70	100.48	91.96	69.54	164.36	258.58
147.74	102.20	93.86	70.47	165.46	137.15
149.75	104.05	95.80	71.40	166.74	128.52
151.73	106.02	97.76	72.33	168.05	127.50
153.70	108.12	99.76	73.28	169.36	128.15
155.64	110.47	Series 17 {msLT(C)}		170.65	129.84
157.45	112.94			171.95	131.50
158.93	115.29	52.15	48.60	173.24	128.71
160.19	117.78	54.10	49.83	ΔH {stabilization; ucHT(B + C*) → sLT(B + C)}	
161.42	121.08	55.96	51.00		
ΔH {stabilization; ucHT(C) → sLT(C)}		57.75	52.11		
		59.48	53.12	Series 2 {sLT(B + C)}	
		61.15	54.10		
		62.77	55.01	236.42	150.08
Series 13 {sHT(C)}		64.35	55.85	239.12	152.12
		65.89	56.69	ΔH {transition; sLT(B + C) → sHT(B + C)}	
257.16	161.83	67.39	57.51		
262.18	165.26	68.85	58.28		
265.27	167.25	70.29	59.01	{sHT(B + C)}	
268.33	169.29	71.70	59.71	263.33	166.26

the opaque crystals still keeping the same crystal size as "A," "C" implies the shattered crystallites, and "C*" means the powdered crystals which have not yet experienced the stable LT-phase. The phase relationship and the change in crystal size have been given in our previous papers.[12,17]

For the sample I, we intended to measure at first the heat capacity of large crystals "A" around the λ-point. Although the specimen was carefully cooled below the λ-point, a disintegration phenomenon suddenly occurred at 154.4 K and the temperature of the calorimeter cell was raised up to 156.5 K. From this temperature rise the heat evolved was determined to be 0.61 kJ mol^{-1}. Since we did not examine whether further fracturings would take place at lower temperatures or not, this value should be regarded as a lower limit of the heat evolution. In spite of the same sieve fraction, the initial disintegration in the calorimeter cell occurred at a temperature about five Kelvin higher than that of DTA. This fact suggests that this phenomenon strongly depends on experimental conditions.

In the case of the sample II, we started the measurement from 162 K and could determine the heat capacities around the λ-point for the large crystals. However, since gradual temperature drift due to the stabilization from the undercooled HT- to the stable LT-phase was observed above 172 K, exact determination of the heat capacity became difficult. Furthermore, an accidental power breakdown in the laboratory made the further measurement impossible. We, therefore, took out the specimen from the cell and loaded sample III freshly prepared.

Sample IV aimed at exact determination of the disintegration heat. The specimen was cooled from 165 K to 10.5 K by controlling the cooling rate as follows; 0.8 K h^{-1} (165–122 K), 2.3 K h^{-1} (122–90 K) and 46.2 K h^{-1} (90–10.5 K). However, since the cooling rate was extremely small at the intial stage, the disintegration was quite incomplete; very small temperature rise due to partial fracturing was sporadically detected at 140.6, 139.4, 134.8, 126.1, 123.2 and 122.6 K. The specimen thus treated consisted of partially shattered crystallites and partially opaque crystals still keeping the initial crystal sizes.

Representative values of the heat capacities are plotted in Figure 3, where the stable phases are shown by open circles and the metastable ones by solid circles. The phase transition between the stable LT- and the stable HT-phase is characterized not only by easy undercooling but also by superheating. Figure 4 illustrates the temperature variation during a continuous heating for the enthalpy measurement of this phase transition (the series 6 of the sample III; designated hereafter as the series III-6 for short). The superheating phenomenon is obvious. In the heat capacity measurements, we could obtain the data of the superheated LT-phase up to 247.66 K (the series III-4) without any disturbance. However, several succeeding points to 247.66 K showed remarkable negative temperature drifts after an energy input, which are due to the stabilization from the superheated LT- to the stable HT-phase. Especially, the ther-

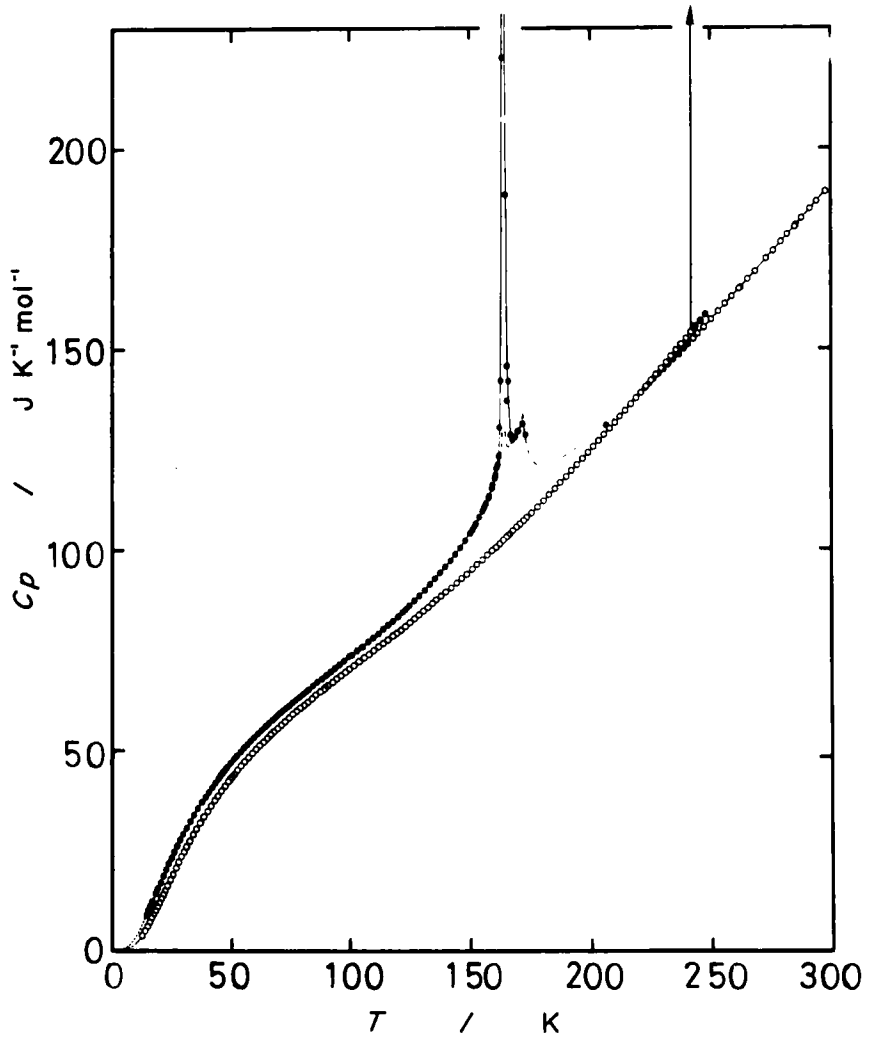

FIGURE 3 Molar heat capacities of ferrocene crystal. O, stable phases; ●, metastable phases; dot-dash curve, metastable phases for large crystals; dotted curve, assumed heat capacities.

mal equilibrium for the point just next to 247.66 K was attained after ten days. Since the final temperature was 242 K, we regarded this as being the most reliable transition temperature. The heat capacities around this phase transition have been given in an enlarged scale in a previous paper.[12]

It is noticeable that the heat capacities measured with different crystal sizes coincide well with one another in a given phase except for the vicinity of the λ-transition at 163.9 K. As shown in Figure 5, the large crystals show sharper heat capacity anomaly than the powdered ones, but the temperature and the

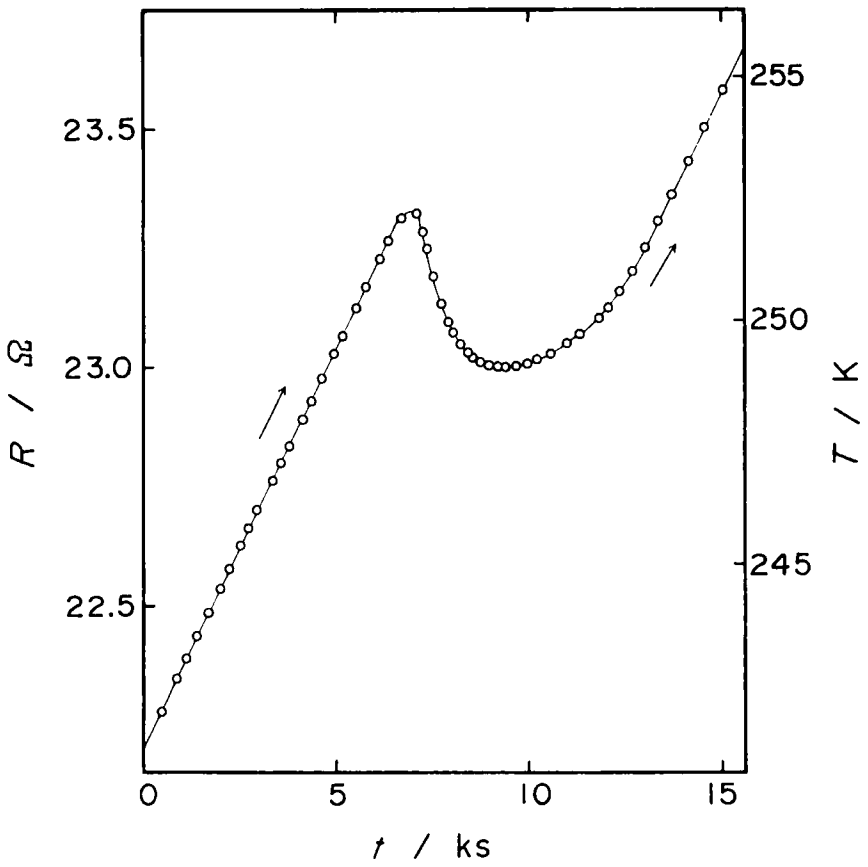

FIGURE 4 Temperature variation during a continuous heating across the phase transition from the stable LT- to the stable HT-phase. A superheating phenomenon is obvious.

enthalpy and entropy of transition agreed well with each other. The results by Edwards *et al.*[1,2] are also reproduced in this figure for comparison. Their values are 2–3 % higher than ours below 180 K and about 5% at room temperature. Contrary to the present study, these authors have succeeded in measuring the heat capaicty of the undercooled HT-phase in the range 180–200 K. In this temperature region, we could not exactly determine the heat capacity because of a spontaneous temperature rise due to the stabilization to the stable LT-phase. Therefore, a quadratic equation of temperature was assumed for the virtual heat capacities in this region and the coefficients were determined based on the enthalpy measurement (the series III-2). The heat capacity thus obtained is given by

$$C_p/\mathrm{J\ K^{-1}\ mol^{-1}} = 300.19 - 2.1431\ (T/\mathrm{K}) + 0.0064074\ (T/\mathrm{K})^2.$$

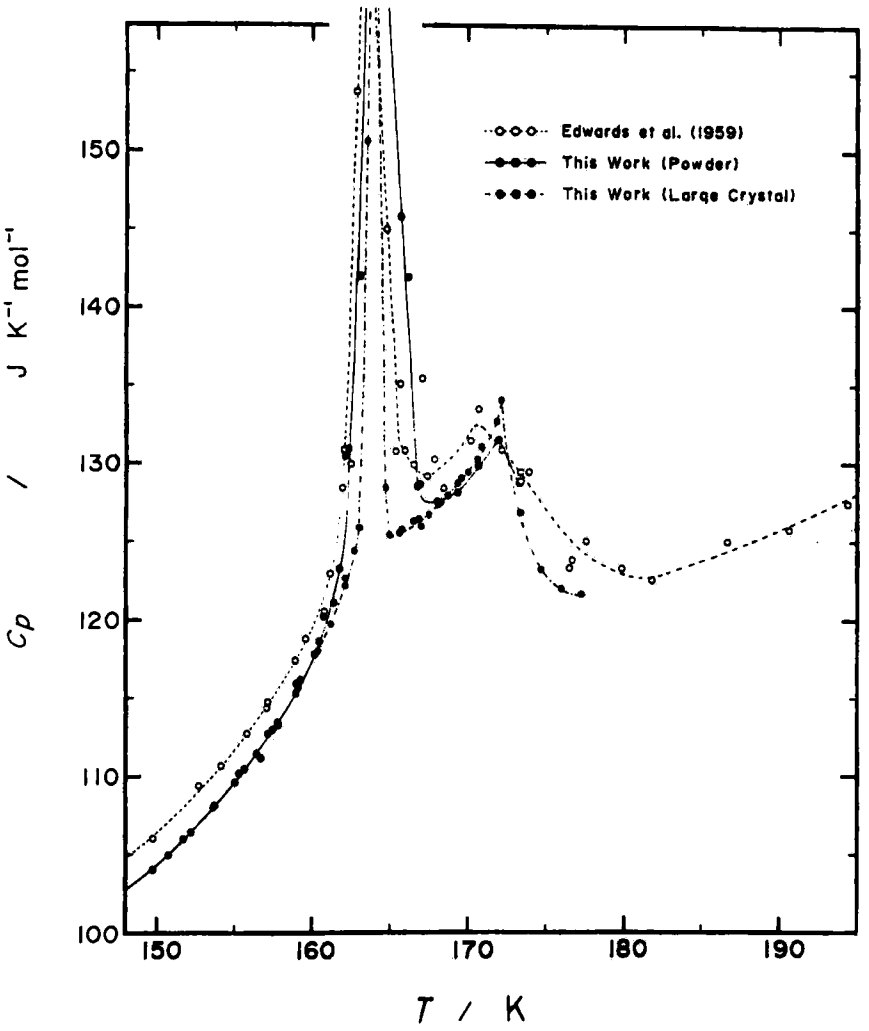

FIGURE 5 Heat capacities of ferrocene crystals around the λ-transition. Dotted curve corresponds to the assumed heat capacity.

The dotted curves in Figures 3 and 5 have been drawn according to this equation.

Enthalpy and entropy of phase transition between stable phases

The enthalpy measurements across the phase transition from the stable LT- to the stable HT-phase at 242 K were made for the opaque crystals (the series III-6), twice for the powdered crystals (the series III-8 and III-10) and for the specimen with mixed crystal sizes (the series IV-2). All the data agreed well

with one another regardless of their crystal sizes. The transition enthalpy was determined to be (4.145 ± 0.005) kJ mol^{-1} as an average of these four measurements. Since this phase transition is of a typical first order and takes place isothermally, the entropy of transition can simply be obtained by dividing the transition enthalpy by the transition temperature to be (17.13 ± 0.02) J K^{-1} mol^{-1}.

Enthalpy and entropy of phase transition between metastable phases

The λ-type transition at 163.9 K with a subsidiary C_p maximum at 169 K is now clearly a phase transition which takes place between the metastable LT- and the undercooled HT-phase. It was originally thought to be of a typical second order[1] while Calvarin and Berar[5] reported a first order nature in the vicinity of the λ-point based on X-ray diffraction analysis. At any rate, as this phase transition exerts its effect over a wide temperature region, say, 120 to 220 K, a "normal" heat capacity which may separate the transition effect from the experimental values should be estimated. To this end, we employed here an effective frequency distribution method,[18] by which the heat capacities below 120 K and above 220 K could be smoothly connected. The enthalpy of transition was determined from the excess area beyond the normal heat capacity curve in the C_p *vs* T diagram to be 0.90 kJ mol^{-1}. On the other hand, the entropy of transition was estimated to be 5.5 J K^{-1} mol^{-1}. We could not find any significant difference between the transition data of the large and powdered crystals. Table II summarizes the data concerning both the stable and the metastable phase transitions, together with the values obtained by Edwards *et al.*[1] for comparison. The present transition data agree well with theirs.

TABLE II

Transition temperature and the enthalpy and entropy of transition for ferrocene crystal

	T_c / K	ΔH / kJ mol^{-1}	ΔS / J K^{-1} mol^{-1}
This work	163.9	0.90	5.5
Edwards *et al.*[1]	163.9	0.854	5.31
This work	242	4.145 ± 0.005	17.13 ± 0.02

Heat of stabilization from metastable to stable phase

The stabilization to the stable LT-phase was found to proceed not only from the undercooled HT-phase but also from the metastable LT-phase below the λ-point although the optimum condition for this stabilization is such that the specimen is annealed at around 190 K after once experiencing the metastable LT-phase.[12] Therefore, the heats of stabilization determined from different

series of measurements should be compared with one another based on the reduced values at a common temperature. For the sake of convenience, we shall choose here 159.56 K for this common temperature. The enthalpy difference between the metastable and the stable LT-phase at 159.56 K, which corresponds just to the heat of stabilization provided that the stabilization would take place at this temperature, was 3.311 kJ mol^{-1} for the large crystals (the series III-3), 3.326 for the opaque crystals (the series III-5), 3.305 and 3.308 for the shattered crystallites (the series III-9 and III-12) and 3.300 for the specimen with mixed crystal sizes (the series IV-1). From these results, the heat of stabilization can be concluded to be independent of crystal size and the averaged enthalpy difference at, say, 159.56 K amounts to (3.310 ± 0.009) kJ mol^{-1}.

Phase relationship

Now that we have gotten all the necessary data, we can make up the phase relationship of ferrocene crystal in terms of any quantities among enthalpy, entropy and Gibbs free energy.

Figure 6 represents the enthalpy diagram, in which the axis of coordinates shows the enthalpy acquisition beyond the zero-point energy of the stable LT-phase, $H^\circ - H_0^\circ$ (stable LT-phase). The enthalpy of the metastable LT-phase at zero Kelvin was found to be larger than that of the stable LT-phase by 2.613 kJ mol^{-1}.

Figure 7 illustrates the entropy diagram. Assuming that the stable LT-phase obeys the third law of thermodynamics, the entropy of the metastable LT-phase at 0 K amounts to 0.17 J K^{-1} mol^{-1}. This value can be regarded as being substantially zero within the present experimental errors. This fact suggests that the triclinic LT-phase hitherto known does not belong to a non-equilibrium state but to a metastable state in which internal equilibrium is attained. Although the molecular packing in the metastable LT-phase seems to be quite different from that in the stable LT-phase, it is of great interest that the molecules are arranged in an ordered state.

The standard thermodynamic functions providing numerical values for the phase relationships are summarized in Tables III and IV for the stable and metastable phases, respectively.

4 DISCUSSION

Edwards *et al.*[1] proposed the mechanism for the λ-type transition in terms of partial rotational disorder of the cyclopentadienyl, C_5H_5, rings in the HT-phase. Based on the fact that the observed entropy of 5.31 J K^{-1} mol^{-1} is very close to R ln 2 (= 5.76 J K^{-1} mol^{-1}), they supposed that two of four possible molecular orientations may be realized in the HT-phase by a gear-wheel

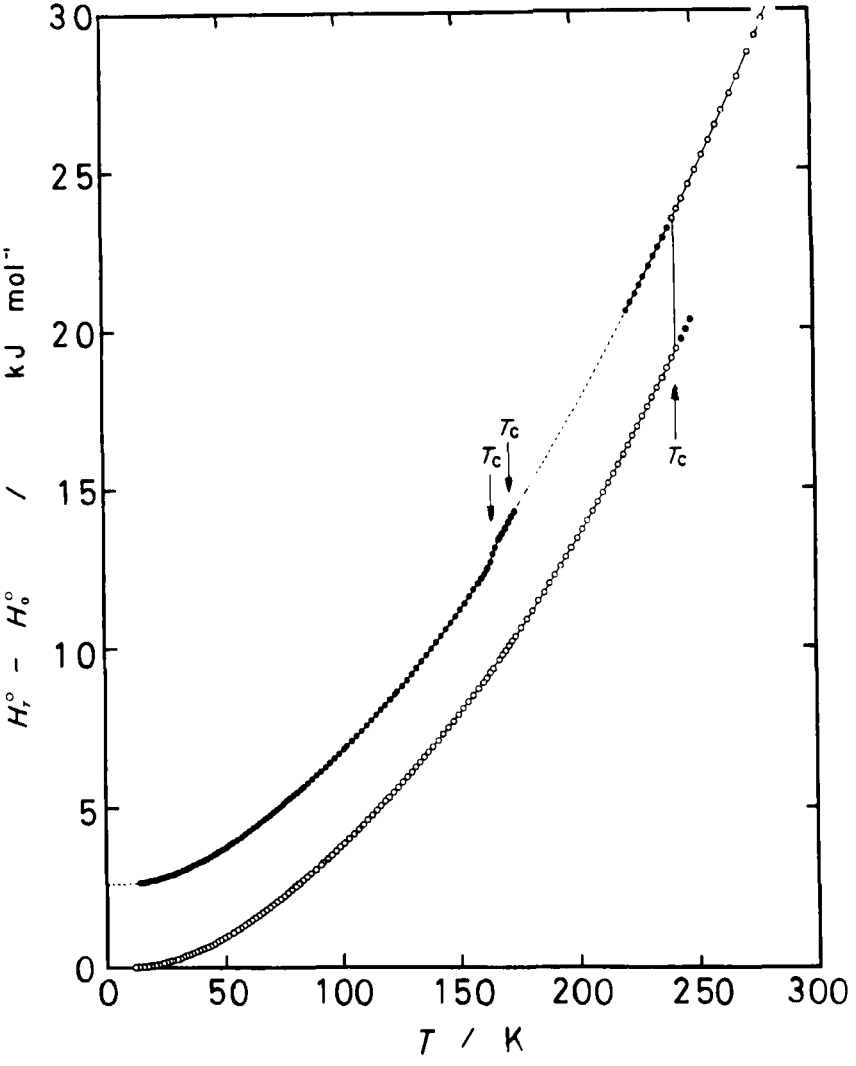

FIGURE 6 Enthalpy relationship among various phases of ferrocene crystal. ○, stable phases; ●, metastable phases.

mechanism of the C_5H_5-array along the crystallographic *c*-axis. The molecular arrangement below the λ-point was imagined to be one of the following three ordered states: (i) all molecules being pentagonal prismatic (eclipsed D_{5h}) in one orientation, (ii) all molecules being pentagonal antiprismatic (staggered D_{5d}) in one orientation or (iii) a mixture of comparatively large regions of D_{5h} molecules surrounding or surrounded by large domains of D_{5d} molecules. Furthermore, their interesting prediction is that another phase transition in

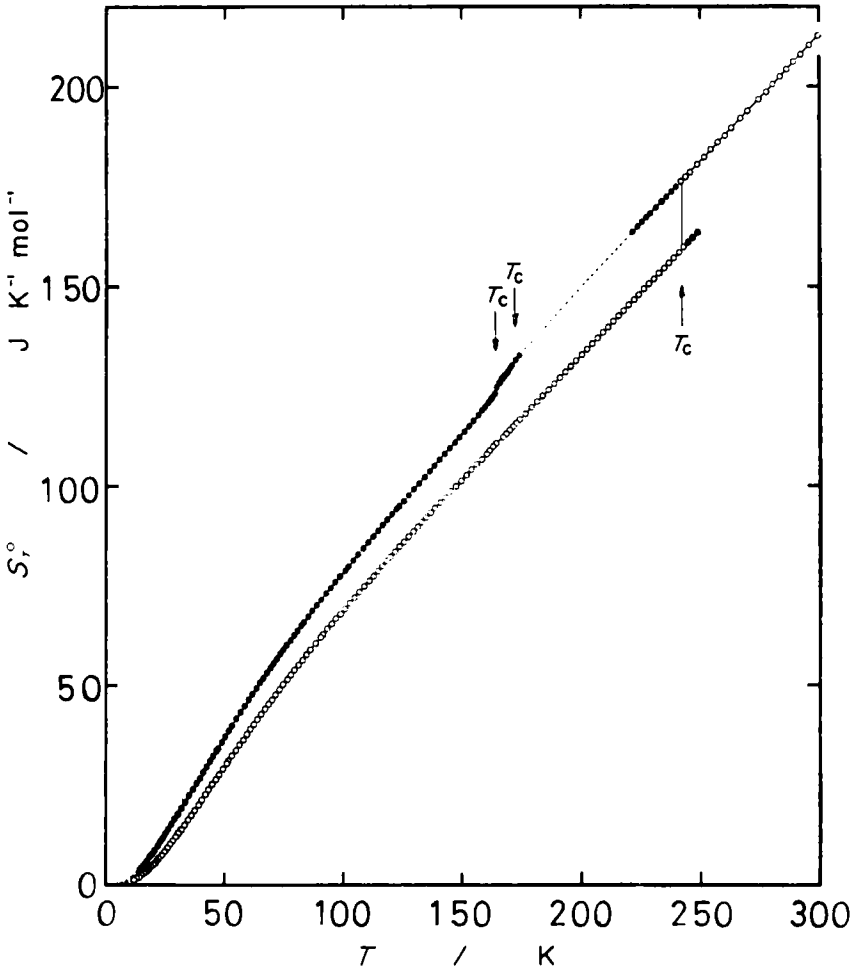

FIGURE 7 Entropy relationship among various phases of ferrocene crystal. ○, stable phases; ●, metastable phases.

which the structure goes to the completely disordered state, with acquiring additional entropy of R ln 2, should be observed above room temperature provided that melting does not intervene.

Although this reorientational model had been supported by many spectroscopic experiments such as IR, Raman, NMR and Mössbauer effect, a few results incompatible with the molecular structure in the LT-phase were also presented as well.[19,20] In particular, definite evidences that disagree with the previous crystal and molecular structures were provided by recent reinvestigations by X-ray[6-9,11] and neutron[10] diffraction analyses. The molecular structures turned out to be neither D_{5d} nor D_{5h} but simply intermediate D_5 in both

TABLE III
Standard thermodynamic functions for the stable phases of ferrocene crystal

T / K	C_p° / J K^{-1} mol^{-1}	S° / J K^{-1} mol^{-1}	$(H^\circ - H_0^\circ)/T$ / J K^{-1} mol^{-1}	$-(G^\circ - H_0^\circ)/T$ / J K^{-1} mol^{-1}
10	(2.16)	(0.73)	(0.55)	(0.18)
20	12.29	4.97	3.63	1.34
30	24.53	12.32	8.60	3.72
40	34.92	20.86	13.93	6.92
50	43.17	29.57	18.99	10.58
60	49.93	38.06	23.60	14.46
70	55.70	46.20	27.78	18.42
80	60.89	53.98	31.60	22.38
90	65.59	61.43	35.12	26.31
100	70.24	68.58	38.40	30.18
110	74.90	75.50	41.51	33.99
120	79.54	82.21	44.48	37.73
130	84.43	88.77	47.37	41.40
140	89.50	95.22	50.20	45.02
150	94.70	101.57	52.99	48.58
160	100.21	107.86	55.77	52.09
170	105.96	114.10	58.55	55.55
180	112.03	120.33	61.36	58.97
190	118.28	126.56	64.19	62.37
200	124.75	132.79	67.05	65.73
210	131.46	139.04	69.96	69.07
220	138.32	145.31	72.92	72.40
230	145.52	151.62	75.92	75.70
240	152.65	157.97	78.97	79.00
250	157.31	181.40	98.57	82.83
260	163.91	187.70	100.95	86.75
270	170.44	194.01	103.01	91.00
280	177.30	200.33	105.54	94.79
290	184.27	206.67	108.13	98.53
300	190.81	213.02	110.78	102.25
273.15	172.61	195.30	103.81	92.19
298.15	189.56	211.85	110.29	101.56

the HT- and the metastable LT-phases. The formally centrosymmetric D_{5d} molecule of the HT-phase can be caused by an averaged superposition of molecules in different orientations randomly distributed throughout the crystal and thus the molecular center of symmetry required by the HT-space group is only statistical in nature.[9,10] Moreover, contrary to the prediction by Edwards *et al.*,[1] the present DSC measurement did not show any anomaly due to further disordering of the C_5H_5-orientations up to the melting point of ferrocene crystal at 173 °C. From these evidences, the mechanism of the λ-transition due to gear-wheel motion of the C_5H_5-rings[1] should be reconsidered.

On the other hand, the entropy of the phase transition at 242 K is as large as 17.13 J K^{-1} mol^{-1} although the high-temperature phase is common to this and the λ-transition. The mechanism of this phase transition cannot be, therefore,

TABLE IV
Standard thermodynamic functions for the metastable phases of ferrocene crystal; H_0° means the enthalpy of the stable low-temperature phase at 0 K

T / K	C_p° / J K^{-1} mol^{-1}	S° / J K^{-1} mol^{-1}	$(H^\circ - H_0^\circ)/T$ / J K^{-1} mol^{-1}	$-(G^\circ - H_0^\circ)/T$ / J K^{-1} mol^{-1}
10	(3.98)	(1.60)	(262.37)	(−260.77)
20	16.76	8.06	136.22	−128.16
30	29.33	17.32	98.57	−81.25
40	39.29	27.19	82.56	−55.37
50	47.10	36.82	74.71	−37.89
60	53.33	45.98	70.66	−24.68
70	58.86	54.64	68.59	−13.95
80	63.79	62.82	67.69	−4.86
90	68.64	70.62	67.53	3.09
100	73.39	78.10	67.88	10.22
110	78.52	85.32	68.59	16.73
120	83.53	92.35	69.62	22.73
130	89.36	99.26	70.90	28.36
140	96.10	106.12	72.46	33.66
150	104.30	113.02	74.30	38.72
160	117.44	120.13	76.54	43.59
170	128.99	129.47	81.10	48.37
180	(122.03)	(136.77)	(83.67)	(53.10)
190	(124.31)	(143.42)	(85.74)	(57.78)
200	(127.87)	(149.88)	(87.75)	(62.13)
210	(132.79)	(156.23)	(89.77)	(66.46)
220	138.58	162.54	91.86	70.68
230	144.61	168.83	94.02	74.81
240	150.73	175.12	96.26	78.86

interpreted only in terms of the reorientational disorder of the C_5H_5-rings ($\approx R \ln 2$). We must have recourse to other mechanisms responsible for reasonable explanation of the excess entropy beyond the orientational entropy; i.e., 11.37 JK^{-1} mol^{-1} (= 17.13 − $R \ln 2$).

A possible mechanism may now be outlined. As shown in Figure 8, a remarkable difference was found between the heat capacities of the metastable and the stable LT-phases even at low temperatures where one need not think of the effect exerted by the λ-transition. This fact strongly suggests that the crystal lattice of the stable LT-phase might be more rigid than that of the metastable LT-phase. This was quite recently confirmed by an X-ray diffraction analysis; the molar volume of the stable LT-phase is much more compact than that of the metastable LT- and the HT-phases (at 250 K, say, $\Delta V/V = 0.023$).[13] Since the molecular packing is more compact in the stable LT-phase, vibrational modes would be expected to shift to the high frequency side. However, the laser Raman spectra did not show any noticeable shifts among the various phases of ferrocene crystal, whereas some characteristic band splittings due to different site symmetries were observed.[17] This fact implies that the inter-

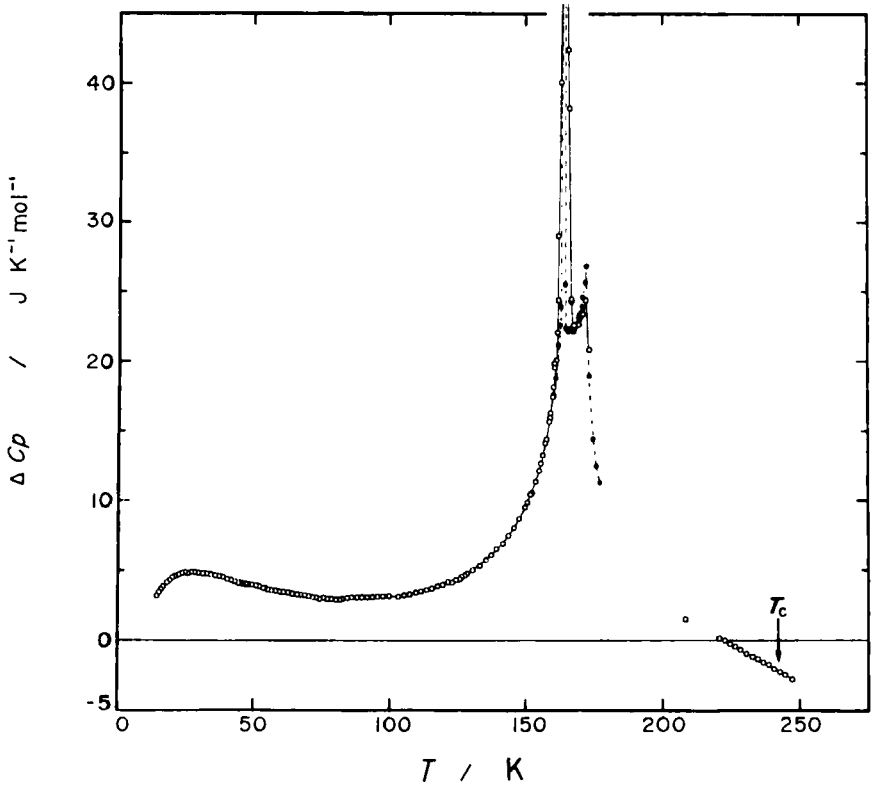

FIGURE 8 Deviation of the heat capacities of the metastable LT- and the undercooled HT-phases from those of the stable LT-phase. ○, powdered crystals; ● and broken lines, large crystals; dotted curve, assumed heat capacities.

atomic distances are substantially identical in all the phases. In other words, the heat capacity difference might be caused not by a change in optical vibrational modes but by a change in acoustic lattice modes.

According to the X-ray diffraction analyses by Edwards *et al.*,[1] and Calvarin and Berar,[5] the thermal expansion coefficient along the *c*-axis is extremely large both in the metastable LT- and the HT-phases. Remarkable anharmonicity of the intermolecular interaction in the *c*-direction is also confirmed by a Mössbauer effect performed by Hill and Debrunner.[21] In order to interpret the large heat capacity difference and the excess entropy of the phase transition at 242 K, we found it very convenient to imagine that the translational mode along the "*c*-axis" in the stable LT-phase would have much higher frequency than that of the metastable LT- and the HT-phases because the former phase is known to be more compact than the latter ones.[13] Figure 9 shows the heat capacities of harmonic oscillators with different wavenumbers from 20 to 100 cm^{-1}. The broken line in this figure represents the heat capacity difference between two oscillators characterized by the wavenumbers of 35

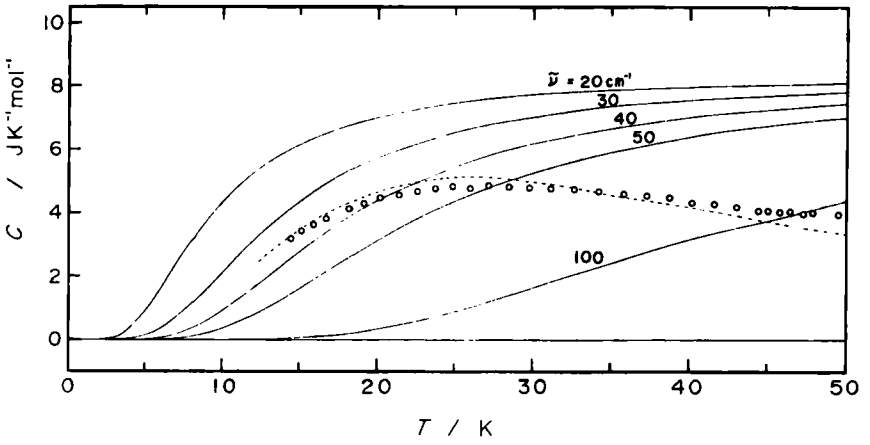

FIGURE 9 Heat capacities of harmonic oscillators with different wavenumbers. Broken line indicates the heat capacity difference between two oscillators characterized by the wavenumbers of 35 and 100 cm^{-1}. Open circles mean the heat capacity difference between the metastable and the stable LT-phase.

and 100 cm^{-1}. This curve was found to reproduce excellently the experimental values at least in the range 13 to 50 K. In addition to this, the entropy difference between these two oscillators at the phase transition point of 242 K amounts to 8.63 J K^{-1} mol^{-1}, which corresponds to about 76% of the excess entropy. The remaining part of the excess entropy would be explained by similar contributions arising from other acoustic modes. From these circumstantial evidences, we incline to conclude that the phase transition between the stable LT- and the HT-phase at 242 K might be accompanied by a softening of the translational mode along the "*c*-axis"; say, from 100 cm^{-1} in the stable LT-phase to 35 cm^{-1} in the HT-phase.

Finally discussed here is the relationship between the strain energy evolved at the disintegration of crystals and the crystal enthalpy acquired thermally. As described in Section 3, a lower limit of the heat evolution due to the disintegration is 0.61 kJ mol^{-1} and in general it is much larger than the enthalpy of the λ-transition (see Figure 2). A question is how this energy is stored in the crystal lattice. Four imaginable cases are schematically given in Figure 10 in terms of the enthalpy diagram. In the case of (a), the strain energy will be produced by partially consuming the enthalpy of the λ-transition. The case (b) is that the enthalpy of the large crystals will be larger than that of the powdered crystals only in the metastable LT- and the HT-phases while there exists no difference between the enthalpies of the λ-transition. The case (c) corresponds to a simple displacement of the enthalpy diagram for the large crystals in the upward direction. In the case of (d), the strain energy will gradually be stored in the lattice with decreasing temperature below the λ-point. However, since the enthalpy of the λ-transition did not show any difference between the large and

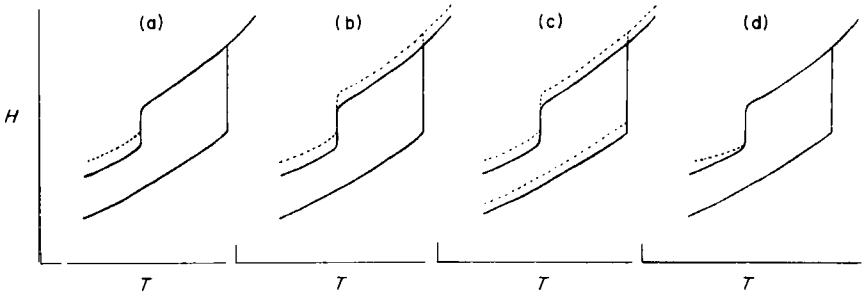

FIGURE 10 Schematic drawing of imaginable enthalpy diagrams for interpretation of the disintegration phenomenon. Broken and solid lines correspond to the large and powdered crystals, respectively.

powdered crystals, the case (a) is immediately excluded. The cases (b) and (c) are also not the case because the enthalpy of stabilization from the metastable to the stable LT-phase was identical regardless of crystal size and also because the heat of fusion determined by the present DSC method was (17.73 ± 0.23) and (17.85 ± 0.10) kJ mol^{-1} for the large and powdered crystals, respectively; indicating no enthalpy difference between the two in the HT-phase. Similarly the last case (d) does not seem to be plausible. If this is the case, the heat capacity of the large crystals should become extremely small below the λ-point because the slope of the enthalpy curve corresponding to the heat capacity is gentle. Although we have not yet measured the heat capacity of the large crystals below 160 K, such a tendency was not detected at all (see Figure 5).

Bodenheimer and Low[14] have reported that the disintegration is not associated with the λ-transition itself but a separate phenomenon which takes place somewhere below the λ-point according to the rate of cooling. This qualitative statement just corresponds to the case (d) and does not account for the real situation.

In any event, the enthalpy diagram under a constant pressure as shown in Figure 10 is not sufficient for interpretation of the disintegration phenomenon. For better understanding, the third variable such as a distortion pressure should be taken into account and the disintegration should be regarded as being a change in the state on a *P-H-T* surface.

References

1. J. W. Edwards, G. L. Kington and R. Mason, *Trans. Faraday Soc.*, **56**, 660 (1960).
2. J. W. Edwards and G. L. Kington, *Trans. Faraday Soc.*, **58**, 1334 (1962).
3. J. D. Dunitz, L. E. Orgel and A. Rich, *Acta Cryst.*, **9**, 373 (1956).
4. J. F. Berar and G. Calvarin, *C. R. Acad. Sci. Paris, Ser. C*, **277**, 1005 (1973).
5. G. Calvarin and J. F. Berar, *J. Appl. Cryst.*, **8**, 380 (1975).
6. G. Clec'h, G. Calvarin, J. F. Berar and R. Kahn, *C. R. Acad. Sci. Paris, Ser. C*, **286**, 315 (1978).
7. J. F. Berar and G. Calvarin, *C. R. Acad. Sci. Paris, Ser. C*, **286**, 581 (1978).

8. G. Clec'h, G. Calvarin, J. F. Berar and D. Andre, *C. R. Acad. Sci. Paris, Ser. C*, **287**, 523 (1978).
9. P. Seiler and J. D. Dunitz, *Acta Cryst.*, **B35**, 1068 (1979).
10. F. Takusagawa and T. F. Koetzle, *Acta Cryst.*, **B35**, 1074 (1979).
11. P. Seiler and J. D. Dunitz, *Acta Cryst.*, **B35**, 2020 (1979).
12. K. Ogasahara, M. Sorai and H. Suga, *Chem. Phys. Lett.*, **68**, 457 (1979).
13. J. F. Berar, G. Calvarin, D. Weigel, K. Chhor and C. Pommier, *J. Chem. Phys.*, **73**, 438 (1980).
14. J. S. Bodenheimer and W. Low, *Phys. Lett.*, **36A**, 253 (1971).
15. H. Suga, H. Chihara and S. Seki, *Nippon Kagaku Zasshi*, **82**, 24 (1961).
16. M. Yoshikawa, M. Sorai, H. Suga and S. Seki, to be published in *J. Phys. Chem. Solids.*
17. M. Sorai, S. Murakawa, K. Ogasahara and H. Suga, *Chem. Phys. Lett.*, **76**, 510 (1980).
18. M. Sorai and S. Seki, *J. Phys. Soc. Japan*, **32**, 382 (1972).
19. Ya. M. Kimel'fel'd, E. M. Smirnova and V. T. Aleksanyan, *J. Mol. Str.*, **19**, 329 (1973).
20. T. C. Gibb, *J. Chem. Soc. Dalton Trans.*, 1237 (1976).
21. C. R. Hill and P. G. Debrunner, *J. Phys. (Paris)*, **37**, C6-41 (1976).